Spatially modulated thermal convection

Marianne Obé
Département Mécanique, Le Madrillet, Institut National des Sciences Appliquées, Saint Etienne du Rouvray, France, and
Roger E. Khayat
Department of Mechanical and Materials Engineering, University of Western Ontario, London, Canada

Received 27 June 2008
Revised 3 November 2008
Accepted 12 January 2009

Abstract

Purpose – The purpose of this paper is to investigate the thermal convection inside a spatially modulated domain.

Design/methodology/approach – The governing equations are mapped onto an infinite strip, allowing Fourier expansion of the flow and temperature in the streamwise direction.

Findings – Similar to Rayleigh-Benard convection, conduction is lost to convection at a critical Rayleigh number, which depends strongly on both the modulation amplitude and the wavenumber. The effect of modulation is found to be destabilizing (stabilizing) for conduction for relatively large (small) modulation wavelength. Oscillatory convection sets in as the Rayleigh number is increased.

Originality/value – This paper presents novel results.

Keywords Convection, Thermal measurement, Oscillation, Wavelengths

Paper type Research paper

1. Introduction

Thermal convection and flow in a micro-channel with modulated walls is a classical problem that has attracted renewed interest because of its immediate relevance to novel micro-technologies, such as compact heat exchangers, and membrane blood oxygenators in extra-corporeal systems (Sobey, 1980). Moreover, the analysis of such flows can help understand the generation of wind waves due to the change in the surface of the earth temperature as well as the atmosphere (Tritton, 1988). The flow can exhibit many of the features present in much more complex geometries, which can significantly impact heat or mass transfer performance. This richness in physical phenomena in a relatively simple geometry motivates fundamental interest by providing an ideal setting to understand pattern formation for both Newtonian and non-Newtonian fluids (Drazin and Reid, 1981).

The effects of spatial wall variations on the steady flow between smooth boundaries were examined only relatively recently. The reader is referred to Zhou *et al.* (2003) for details and bibliography therein. One may refer to such variations from perfect geometries as dirty effects. On the other hand (Schmitz and Zimmerman, 1996a), these deviations can lead to interesting phenomena, which are not present in systems of regular geometrical variation. Sidewalls, for example, may restrict the structure of stable wave numbers for cellular patterns or modify the orientation of convection rolls (Schmitz and Zimmerman, 1996b; Stork and Miller, 1972; Thompson *et al.*, 1985). Reflection effects (Cross, 1988) or dynamical structures (Ning and Ecke, 1993) can be induced in systems like rotating Rayleigh-Bénard convection. Irregularities at the boundaries may lead to localized cellular structures at the threshold of convection,

The support of the Natural Science and Engineering Research Council of Canada, and that of the Institut National des Sciences Appliquées de Rouen, is gratefully acknowledged.

International Journal of Numerical Methods for Heat & Fluid Flow
Vol. 20 No. 1, 2010
pp. 17-36

0961-5539
DOI 10.1108/09615531011008109

similar to those of gravity waves (Dimitropoulos *et al.*, 1998). Such phenomena modify the bifurcation behavior of cellular structures, as shown for a model system (Zimmerman *et al.*, 1993).

To gain insight on the effects of roughness in pattern formation, it is often helpful to have it replaced with periodic modulations. One may replace, for instance, imperfections at the boundaries in convection by temperature variations and analyze their consequences for the onset of convection. Davis (1976) studied the case of temporal periodic variations. Kelly and Pal (1978) examined the effects of spatially periodic boundary conditions on the stability of the Rayleigh-Bénard problem. Chen and Whitehead (1968) evaluated the extent to which well-defined initial perturbations affect stable boundaries, although they were steady in time. The practical value is that one might want to make the boundary wavy if the mean Nusselt number could be increased, which have motivated Watson and Poots (1971) to study the effects of wavy boundaries on laminar free convection in a flow between parallel vertical walls.

Other modulated systems have also been examined by Khayat and co-workers, such as the flow through sinusoidally shaped channels. Steady flow (Zhou *et al.*, 2002, 2003), as well as stability aspects were considered (Selvarajan *et al.*, 1999; Szumbarski and Floryan, 1999). One of the major difficulties compared to typical linear stability analyses is the absence of analytical solution for the base flow analyzed. This is also the case for modulated rotating flow, of closer relevance to the current problem of thermal convection. Li and Khayat (2004) showed the existence of intricate steady pattern formation, but limited their formulation to weakly modulated Taylor-Couette flow. Finite amplitude forcing was later considered by Zhang and Khayat (2006). This problem may be viewed as the counterpart to the current problem in modulated thermal convection.

Pattern formation is related to finite size or inhomogeneity effects. In this work, the effect of spatial modulation on steady conduction and thermal convection, as well as their stability are examined. The flow and temperature fields are obtained by mapping the physical domain onto the rectangular computation domain, and using a combined Galerkin projection and spectral methodology. The influence of the Rayleigh number, dimensionless wave number and amplitude on the flow and heat transfer is emphasized.

2. Problem formulation and solution procedure

In this section, the general equations and boundary conditions for the transient and steady-state flow of a Newtonian fluid in a spatially modulated channel are presented. The equations are mapped over a rectangular domain, reducing the problem.

2.1 Governing equations and boundary conditions

Consider the flow of an incompressible Newtonian fluid lying horizontally between two infinite rigid stationary boundaries, the lower being straight and the upper periodically modulated. Let T_0 and $T_0 + \delta T$ be the temperatures of the upper and lower plates, respectively, with δT being the temperature difference. The problem is first introduced in the (X, Z) plane, with the X-axis taken along the lower wall and the Z-axis along the direction perpendicular to the plates. The general shapes of the lower and upper plates are given by $Z = 0$ and $D + F(X)$, respectively, where D is a typical (mean) channel height and F(X) is a general function of X that may be arbitrarily prescribed. In this work, however, a sinusoidal modulation will be considered. Figure 1 illustrates schematically the flow configuration, with dimensionless notations being used. The current formulation is easily extended to other configurations, such as the modulation

of both the lower and upper plates, sinusoidally or otherwise, as long as the modulation is periodic in X.

The fluid is assumed to be incompressible of density ρ and viscosity μ. In this study, the Boussinesq approximation is assumed to hold, which states that the effect of compressibility is negligible everywhere in the conservation equations except in the buoyancy term, i.e. that density differences are sufficiently small to be neglected, except where they appear in terms multiplied by **g**, the acceleration due to gravity. The fluid of main interest is assumed to obey the following equation of state:

$$\rho = \rho_0[1 - \alpha_T(T - T_0)], \tag{1}$$

where ρ_0 is the density at T_0 and α_T is the coefficient of volumetric expansion. In this case, the equations for conservation of mass, momentum and energy read, respectively:

$$\begin{aligned} &\nabla \cdot \mathbf{U} = 0, \\ &\rho_0(\mathbf{U}_s + \mathbf{U} \cdot \nabla \mathbf{U}) = -\nabla P + \mu \nabla^2 \mathbf{U} + \rho \mathbf{g}, \\ &T_S + \mathbf{U} \cdot \nabla T = \kappa \nabla^2 T, \end{aligned} \tag{2}$$

where **U**(U,W) is the velocity vector, ∇ is the two-dimensional gradient operator, S is time, P is the hydrostatic pressure, **g** is the acceleration vector due to gravity, κ is the thermal diffusivity and T is the temperature. The subscript S denotes partial differentiation with respect to time. The two boundaries are treated as slip surfaces. The dimensionless co-ordinates, x and z, time, t and velocity components, u and w, are introduced as:

$$x = \frac{X}{D}, \quad z = \frac{Z}{D}, \quad t = \frac{\kappa}{D^2}S, \quad u = \frac{DU}{\kappa}, \quad w = \frac{DW}{\kappa}, \tag{3a}$$

while the departures in temperature, θ, and pressure, p, from the pure conduction state temperature, T_{SS}, and pressure, P_{SS}, as well as the temperature departure, ω, from T_0, are given by:

$$\theta = \frac{T - T_{ss}}{\delta T}, \quad p = \frac{D^2}{\mu\kappa}(P - P_{ss}), \quad \omega = \frac{T_{ss} - T_0}{\delta T}. \tag{3b}$$

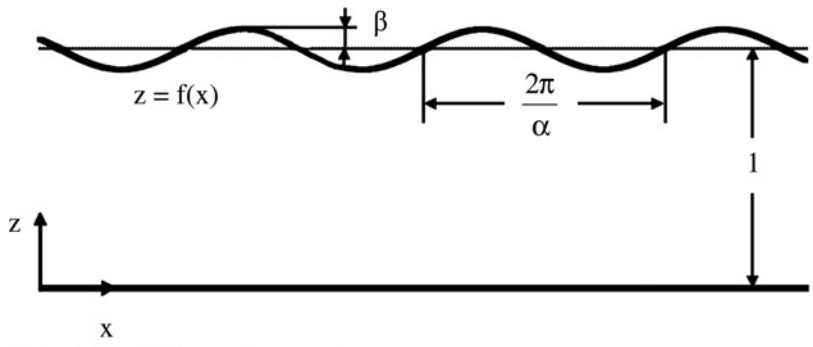

Note: All variables are dimensionless

Figure 1.
Schematic illustrating the physical domain and thermal convection between straight lower plate and spatially modulated upper plate

Here, pure conduction is referred to the state of the fluid at rest. In this case, P_{SS} is of hydrostatic character. Two dimensionless groups emerge in the problem, namely, the Rayleigh number and the Prandtl number:

$$\mathrm{Ra} = \frac{\delta T \rho_0 g \alpha_T D^3}{\mu \kappa}, \quad \mathrm{Pr} = \frac{\mu}{\rho_0 \kappa}. \tag{4}$$

In this case, Equations (2) reduce to:

$$\begin{aligned} &u_x + w_z = 0, \\ &u_t + uu_x + wu_z = \mathrm{Pr}(\Delta u - p_x), \\ &w_t + uw_x + ww_z = \mathrm{Pr}(\Delta w - p_z + \mathrm{Ra}\theta), \\ &\theta_t + u(\theta + \omega)_x + w(\theta + \omega)_z = \Delta\theta, \end{aligned} \tag{5}$$

where a subscript denotes partial differentiation. Note that $\omega(x, z)$ is governed by Laplace's equation. The problem (5) is defined over the physical domain $\Omega_{xz} = \{(x, z) | x \in [0, 2\pi/\alpha], z \in [0, 1 + f(x)]\}$, which is next mapped onto the rectangular domain. The physical domain and flow configuration are schematically illustrated in Figure 1. Here $f(x) = \beta \sin(\alpha x)$ is the deviation in the modulated upper boundary from its mean value, with α and β being the wavenumber and amplitude (normalized by D^{-1} and D), respectively.

2.2 Domain transformation

In contrast to the convection between flat plates, the flow and the temperature in the current situation are not periodic in the streamwise direction given the competition between the imposed modulation of wavenumber α and the "natural" or spontaneous disturbance of wavenumber k. However, if the problem is solved over an infinite strip of constant height, the flow and the temperature variables can still be taken as Fourier series in the streamwise direction with basic wavenumber k. For this, the periodic physical domain Ω_{xz} is mapped onto the rectangular domain $\Omega_{\xi\eta} = \{(\xi, \eta) | \xi \in [0, 2\pi/\alpha], \eta \in [0, 1]\}$ following the transformation:

$$\tau(x, z, t) = t, \quad \xi(x, z, t) = x, \quad \eta(x, z, t) = \frac{z}{1 + f}. \tag{6}$$

Applying the transformations, Equations (5) become:

$$u_\xi - \eta \frac{f'}{1+f} u_\eta + \frac{1}{1+f} w_\eta = 0, \tag{7a}$$

$$\begin{aligned} &u_\tau + u\left(u_\xi - \eta \frac{f'}{1+f} u_\eta\right) + w \frac{1}{1+f} u_\eta \\ &\quad = \mathrm{Pr}\left[\begin{aligned} &\eta\left(-\frac{f''}{1+f} + 2\left(\frac{f'}{1+f}\right)^2\right) u_\eta - 2\eta \frac{f'}{1+f} u_{\eta\xi} + u_{\xi\xi} \\ &+ \eta^2 \left(\frac{f'}{1+f}\right)^2 u_{\eta\eta} + \left(\frac{1}{1+f}\right)^2 u_{\eta\eta} - \left(p_\xi - \eta \frac{f'}{1+f} p_\eta\right) \end{aligned}\right], \end{aligned} \tag{7b}$$

$$w_\tau + u\left(w_\xi - \eta\frac{f'}{1+f}w_\eta\right) + w\frac{1}{1+f}w_\eta = \mathrm{Pr}\left[\begin{array}{l}\eta\left(-\dfrac{f''}{1+f} + 2\left(\dfrac{f'}{1+f}\right)^2\right)w_\eta - 2\eta\dfrac{f'}{1+f}w_{\eta\xi} + w_{\xi\xi} \\ +\eta^2\left(\dfrac{f'}{1+f}\right)^2 w_{\eta\eta} + \left(\dfrac{1}{1+f}\right)^2 w_{\eta\eta} - \dfrac{1}{1+f}p_\eta + \mathrm{Ra}\theta\end{array}\right], \tag{7c}$$

$$\theta_\tau + u\left(\theta_\xi - \eta\frac{f'}{1+f}\theta_\eta\right) + w\frac{1}{1+f}\theta_\eta + u\left(\omega_\xi - \eta\frac{f'}{1+f}\omega_\eta\right) + w\frac{1}{1+f}\omega_\eta = \eta\left(-\frac{f''}{1+f} + 2\left(\frac{f'}{1+f}\right)^2\right)\theta_\eta - 2\eta\frac{f'}{1+f}\theta_{\eta\xi} + \theta_{\xi\xi} + \left(\frac{1}{1+f}\right)^2[(\eta f')^2 + 1]\theta_{\eta\eta}, \tag{7d}$$

Regarding the boundary conditions, no penetration condition is assumed to hold at the two bounding surfaces regardless of the nature of the surfaces. In other words, the surfaces are assumed to be impermeable. The temperature is assumed fixed at the two surfaces. In this work, the two boundaries are assumed to be slip surfaces. Although less realistic than the rigid-rigid conditions, the free-free conditions adopted here have been extensively used in the literature on Rayleigh-Benard convection as they allow the expansion of the flow and temperature fields in terms of trigonometric functions in the transverse direction. More importantly, one does not expect any qualitative difference in flow behavior if one set of conditions or the other are used. Indeed, Khayat (1999) confirmed this similarity in behavior for Taylor-Couette flow. For this reason, the free-free conditions are used here since the current formulation and results collapse onto those for the traditional Rayleigh-Benard convection in the limit of flat bounding surfaces. Thus, the boundary conditions at the top and bottom boundaries for velocity and departure in temperature reduce to:

$$\begin{aligned}&u_\eta(\xi, \eta = 0, \tau) = w(\xi, \eta = 0, \tau) = \theta(\xi, \eta = 0, \tau) \\ &\quad = u_\eta(\xi, \eta = 1, \tau) = w(\xi, \eta = 1, \tau) = \theta(\xi, \eta = 1, \tau) = 0.\end{aligned} \tag{8a}$$

In addition, periodic conditions are imposed in the streamwise direction, or:

$$\begin{aligned}&u(\xi, \eta, \tau) = u\left(\xi + \frac{2\pi}{k}, \eta, \tau\right), \quad w(\xi, \eta, \tau) = w\left(\xi + \frac{2\pi}{k}, \eta, \tau\right), \\ &\theta(\xi, \eta, \tau) = \theta\left(\xi + \frac{2\pi}{k}, \eta, \tau\right),\end{aligned} \tag{8b}$$

where k is a wave number to be specified later. Finally, the pure conduction state is governed by:

$$\omega_{\xi\xi} + a^2[(\eta f')^2 + 1]\omega_{\eta\eta} - 2\eta a f'\omega_{\xi\eta} + \eta[2(af')^2 - af'']\omega_\eta = 0, \tag{9}$$

subject to $\omega(\xi, \eta = 0) = 1$ and $\omega(\xi, \eta = 1) = 0$. In addition to the conditions at the two boundaries, periodic conditions will be used. In this case, $\omega(\xi, \eta) = \omega(\xi + (2\pi/\alpha), \eta)$. The problem is now solved using a combined spectral/Galerkin approach.

2.3 Solution for the conduction state

A Galerkin projection method is used to solve the problem. The solution corresponding to pure conduction is expressed in Fourier series of fundamental wavelength equal to $2\pi/\alpha$. Thus:

$$\omega(\xi, \eta) = \sum_{n=0}^{N} [A_n^c(\eta) \cos n\alpha\xi + B_n^s(\eta) \sin n\alpha\xi], \tag{10}$$

which, upon substituting in Equation (9) and projecting over the interval $\xi \in [0, 2\pi/\alpha]$, lead to a set of ordinary differential equations for the coefficients, which must be solved subject to $A_0^c(0) = 1, A_{n>0}^c(0) = B_{n>0}^s(0) = 0$ and $A_{n\geq 0}^c(1) = B_{n>0}^s(1) = 0$. Reasonable convergence is reached by including only a few modes. The following equations are given for the coefficients corresponding to $N = 1$:

$$\begin{aligned}
A_{\eta\eta}^0 &= \frac{1}{(\eta ß\alpha)^2 + 2}[-3\eta(ß\alpha)^2 A_\eta^0 + 2ß\alpha^2 B^s + \eta ß\alpha^2 B_\eta^s], \\
A_{\eta\eta}^c &= \frac{1}{3(\eta ß\alpha)^2 + 4}[\alpha^2(ß^2 + 4)A^c - 9\eta(ß\alpha)^2 A_\eta^c], \\
B_{\eta\eta}^s &= \frac{1}{(\eta ß\alpha)^2 + 4}[-4\eta ß\alpha^2 A_\eta^0 + \alpha^2(3ß^2 + 4)B^s - 3\eta(ß\alpha)^2 B_\eta^s].
\end{aligned} \tag{11}$$

Note in this case that $A^0 = A_0^c, A^c = A_1^c, B^s = B_1^s$. System (11) is solved as a two-point boundary-value problem using a finite-difference scheme with deferred correction, coupled with a modified Newton-Raphson method (see, for instance, Rangan, 2003 for details).

2.4 Solution procedure for the convection state

For convection, the solution is sought by expanding the velocity, pressure and temperature as Fourier series in ξ, of fundamental wavenumber k, with the expansion coefficients depending on η (and time). Thus, the flow and temperature fields are assumed to be periodic in the ξ direction with wavelength $2\pi/k$:

$$\begin{aligned}
u(\xi, \eta, \tau) &= U^0(\eta, \tau) + U^c(\eta, \tau)\cos(k\xi) + U^s(\eta, \tau)\sin(k\xi), \\
w(\xi, \eta, \tau) &= W^0(\eta, \tau) + W^c(\eta, \tau)\cos(k\xi) + W^s(\eta, \tau)\sin(k\xi), \\
p(\xi, \eta, \tau) &= P^0(\eta, \tau) + P^c(\eta, \tau)\cos(k\xi) + P^s(\eta, \tau)\sin(k\xi), \\
\theta(\xi, \eta, \tau) &= \theta^0(\eta, \tau) + \theta^c(\eta, \tau)\cos(k\xi) + \theta^s(\eta, \tau)\sin(k\xi).
\end{aligned} \tag{12}$$

Upon substitution into Equations (7) and projecting onto the various modes, a set of coupled partial differential equations are obtained, which are given in the Appendix. The steady-state coefficients are obtained using a finite difference method in η similar to above. Unlike the convection between two flat plates, only a few modes are needed in

order to preserve all the nonlinearities. The method of solution follows closely that of Zhang and Khayat (2006), and will therefore not be discussed here.

It is important to emphasize that while the temperature field (10) for pure conduction has the same spatial periodicity as the geometrical modulation of the upper plate, the convective field (12) is not commensurate with the plate modulation. In fact, it is not difficult to conclude, upon inspecting transformation (6) and expansions (12), that the convective field has no spatial periodicity.

3. Results and discussion

In this section, steady convection patterns and their stability are analyzed for different flow and geometrical parameters. Similarly to Rayleigh-Benard convection between two flat plates, steady conduction loses its stability to steady convection at a critical Rayleigh number, Ra_C, which depends not only on the disturbance wavenumber k, but also on the modulation wavenumber, α, and amplitude, β. As the Rayleigh number increases, the steady convective pattern loses its stability in turn to oscillatory convection at a Rayleigh number Ra_H. In the sequel, it is convenient to introduce the modulation wavelength $\lambda_\alpha \equiv 2\pi/\alpha$ and the disturbance wavelength $\lambda_k \equiv 2\pi/k$.

Consider first pure conduction, which will be taken as reference later on. Figure 2 illustrates typically the temperature distribution in the modulated domain over one wavelength. The figure shows the influence of modulation amplitude, β for $\alpha = 1$. Note in this case that the solution has the same wavelength as that of the imposed modulation. In the absence of modulation ($\beta = 0$), the temperature distribution is of course linear. As β increases, a nonlinear temperature distribution emerges, with a temperature gradient larger near the upper plate than at the bottom.

3.1 Modulation at low wavenumber

The influence of modulation amplitude, β, is shown in Figure 3 for $Pr = 10$, modulation and flow wavenumbers $\alpha = 1$ and $k = \pi/\sqrt{2}$, respectively. Both the flow field and temperature contours are depicted. Note that for this modulation wavenumber the critical disturbance wavenumber for any modulation amplitude is very close to that corresponding to the convection between two flat plates, therefore the choice of the above k value in this case (see below). The patterns in Figure 3 are plotted over one modulation wavelength, in this case $x \in [0, \lambda_\alpha = 2\pi]$. Clearly, the flow and temperature patterns do not change in periodicity even under large modulation amplitude (as for $\beta = 0.9$). The convection pattern becomes simply distorted due to the expansion and contraction resulting from modulation. However, it is interesting to note the loss of the warm (bright) regions, which decrease essentially by half relative to the $\beta = 0$ case (see Figure 3 for $\beta = 0.9$).

The rate of heat transfer is significantly influenced by modulation. Figure 4 displays the dependence of the local Nusselt number, Nu(x), on the modulation amplitude for the same parameters as in Figure 3. Note that $Nu(x) = 1 - (\partial\theta/\partial z)|_{z=0}$. It is interesting to observe that the response in convection rate is highly nonlinear with respect to modulation amplitude. The figure shows that the rate of convection is essentially unaffected by modulation amplitude for $\beta < 0.6$. At larger amplitude, there is a significant increase in convection rate resulting from domain contraction (see Figures 3 and 4 for $\beta = 0.9$). In contrast, there is barely any change in Nu(x) over the range $0 < x < \pi$, where considerable domain expansion has occurred. The influence of modulation amplitude on the overall rate of convection is depicted in Figure 5, where the Nusselt number, $\langle NU(x) \rangle$, averaged over a wavelength is plotted against Ra for

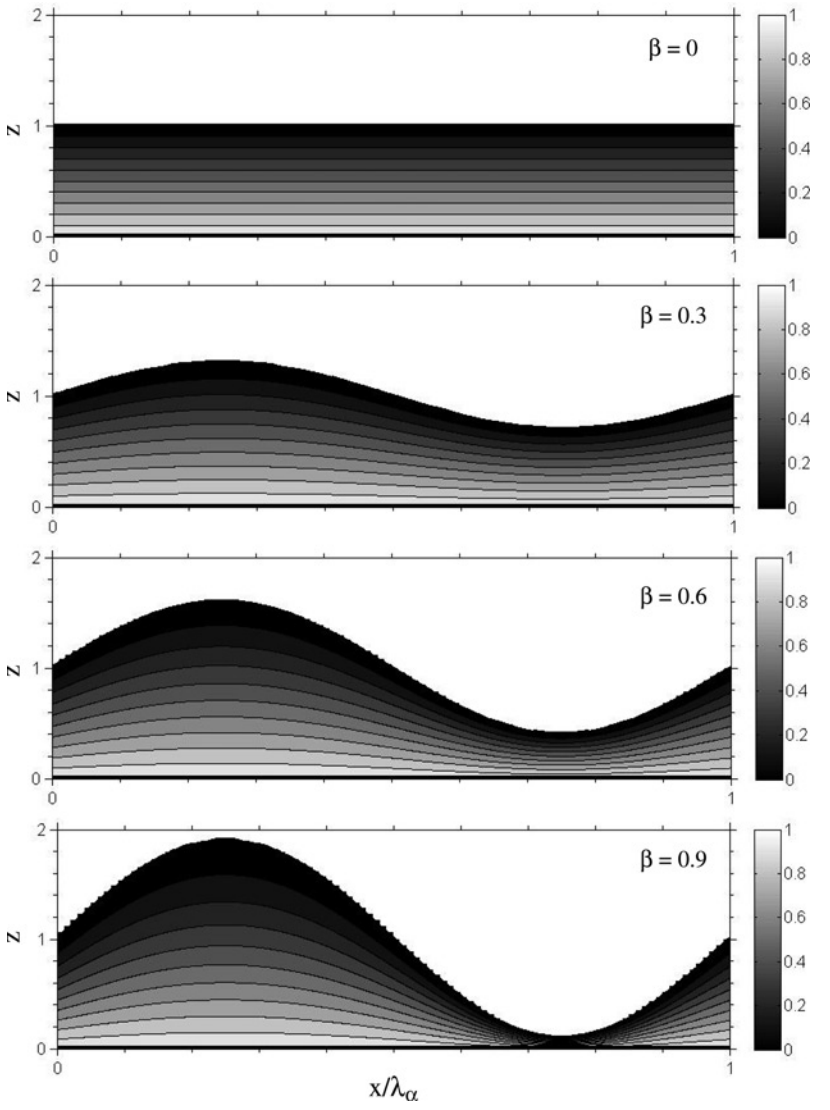

Figure 2.
Temperature distribution of the pure conduction state over one modulation wavelength, $x \in [0, 2\pi]$, for $Ra = 200$, $\alpha = 1$ and $Pr = 10$

$\alpha = 1$. The curves in Figure 5 reflect simultaneously the bifurcation picture as the exchange in stability between conduction and convection takes place at the critical Rayleigh number. The figure shows that the overall rate of convection tends to increase with modulation amplitude as the critical Rayleigh number decreases, albeit nonmonotonically. Thus, modulation tends to enhance the onset and magnitude of convection.

The corresponding marginal stability curves are shown in Figure 6, where the critical Rayleigh number, Ra_C, is plotted against k for different β values. The curves are plotted over the range $0 \leq Ra \leq 7{,}000$ in Figure 6a and $250 \leq Ra \leq 1{,}000$ in Figure 6b. Figure 6a suggests that the overall range of stability of the conduction state

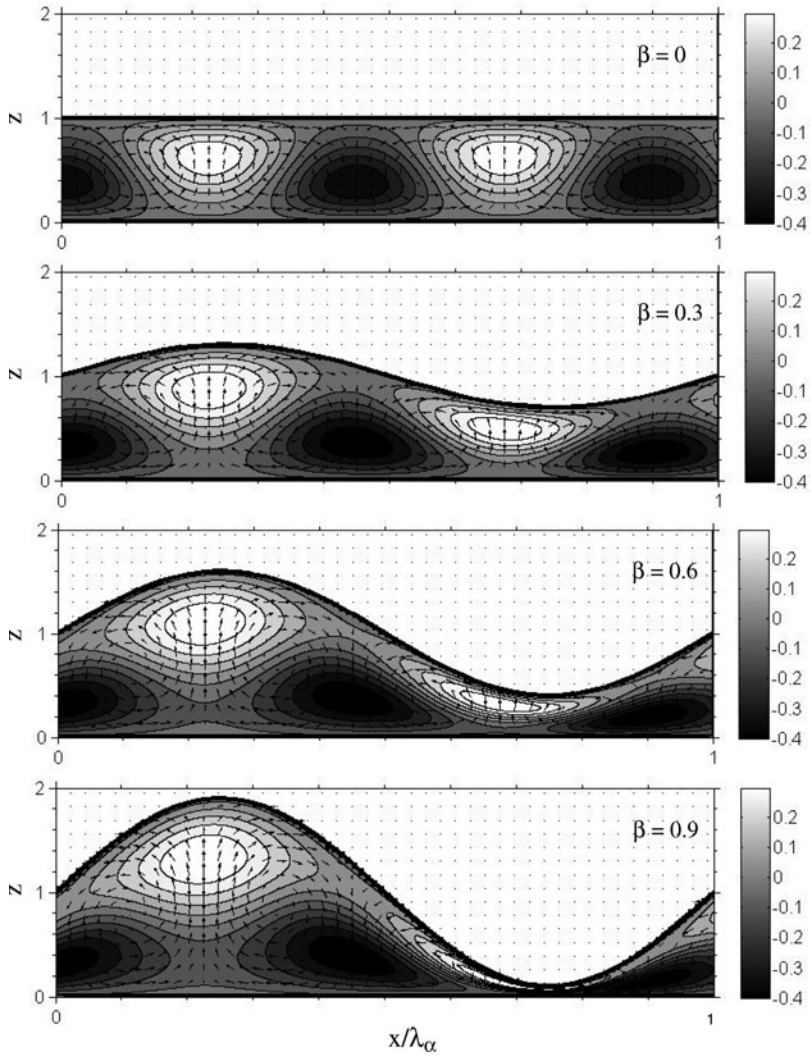

Figure 3.
Influence of modulation amplitude ß on flow and temperature over one modulation wavelength, $x \in [0, 2\pi]$, for $Ra = 900$, $\alpha = 1$, $Pr = 10$ and $k = \pi/\sqrt{2}$

increases with modulation amplitude. This is particularly obvious from the small k range. In this range, a second and sharper minimum appears for $\beta > 0$. For large k, the stability picture is essentially uninfluenced by β. While the minimum critical Rayleigh number, $Ra_c^m \equiv Ra_c(k_m)$, depends significantly on modulation amplitude, the corresponding wavenumber, k_m, remains close to $k = \pi/\sqrt{2}$. This is confirmed by the locus of minimum values shown in Figure 6b. As the Rayleigh number increases beyond Ra_C, steady convection is lost to oscillatory convection (via a Hopf bifurcation) at a critical Rayleigh number Ra_H.

Figure 7 shows the dependence of the critical thresholds for the onset of steady convection (Figure 7a) and oscillatory convection (Figure 7b), along with the corresponding oscillatory frequency (Figure 7c). Here $k = \pi/\sqrt{2}$ and $\alpha = 1$. Figure 7 illustrates the range of stability of steady convection, i.e. for $Ra_c < Ra < Ra_H$. Figure

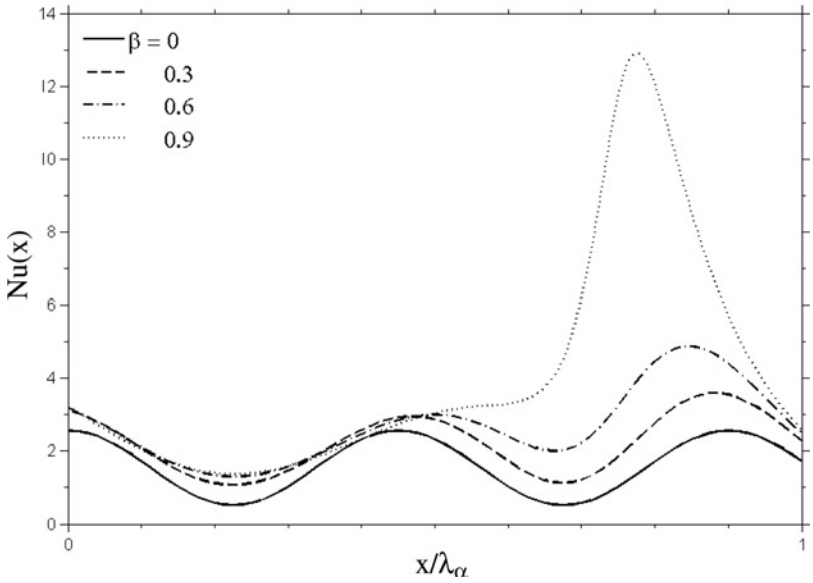

Figure 4.
Influence of modulation amplitude on the distribution of the Nusselt number over one modulation wavelength, $x \in [0, 2\pi]$, for $Ra = 900$, $\alpha = 1$, $Pr = 10$ and $k = \pi/\sqrt{2}$

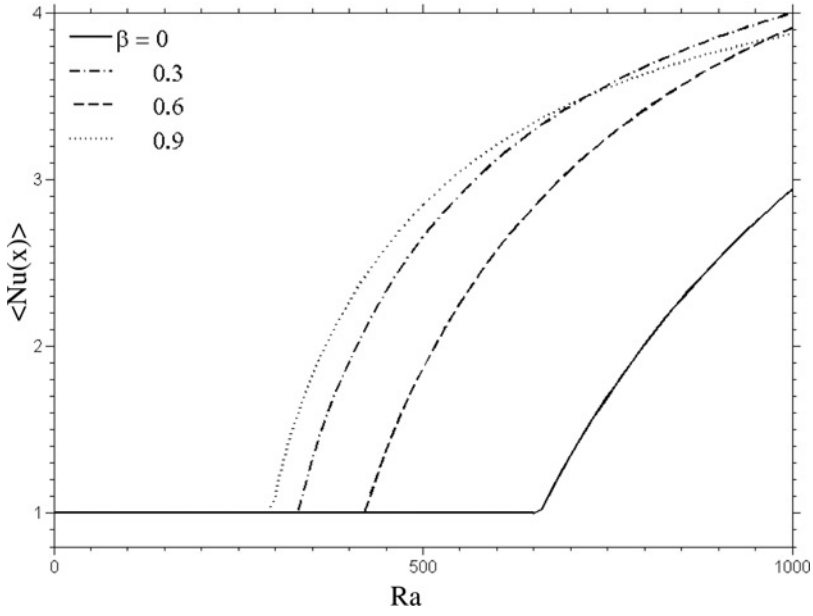

Figure 5.
Influence of modulation amplitude on the overall Nusselt number for $\alpha = 1$, $Pr = 10$ and $k = \pi/\sqrt{2}$

7a shows that Ra_c decreases with modulation amplitude roughly following $Ra_c = -267 \log \beta + 284$. Figure 7b shows the variation of Ra_H, which also decreases with β at approximately the same rate as Ra_c, following $Ra_H = -7{,}694 \log \beta + 4{,}006$. Thus, it seems that the range of stability $Ra_c < Ra < Ra_H$ is essentially unaffected by

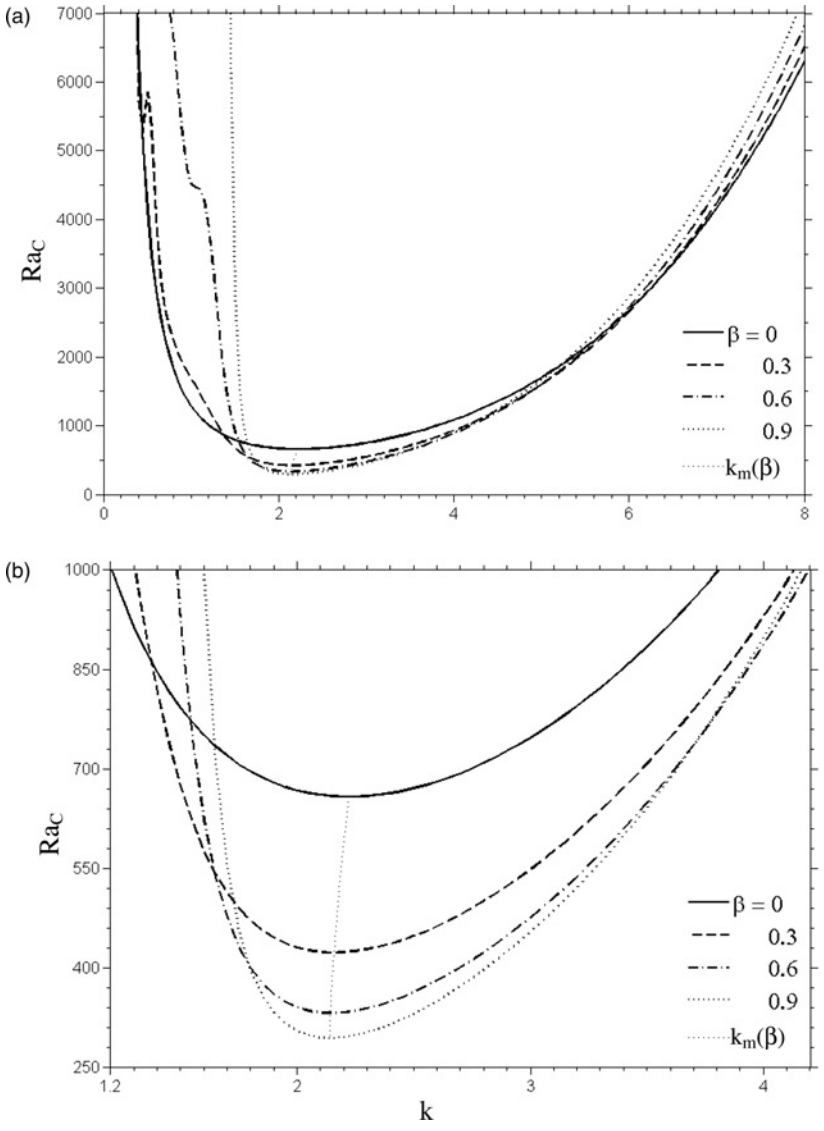

Figure 6.
Influence of modulation amplitude on the neutral stability curves corresponding to the loss of stability of pure conduction and the onset of thermal convection, over two different ranges of critical Rayleigh number (Figures 6a and b) for $\alpha = 1$

domain modulation. The corresponding distribution of the frequency is given in Figure 7c, which indicates that oscillatory convection sets in at a frequency that decreases with modulation amplitude.

3.2 Modulation at high wavenumber

For small modulation wavenumber, the response of the flow and heat transfer is rather commensurate with modulation amplitude. Thus, in general, convection is enhanced by the amplitude. As will now be reported, this is not the case at high modulation wavenumber. Consider first the dependence of the convection patterns displayed in

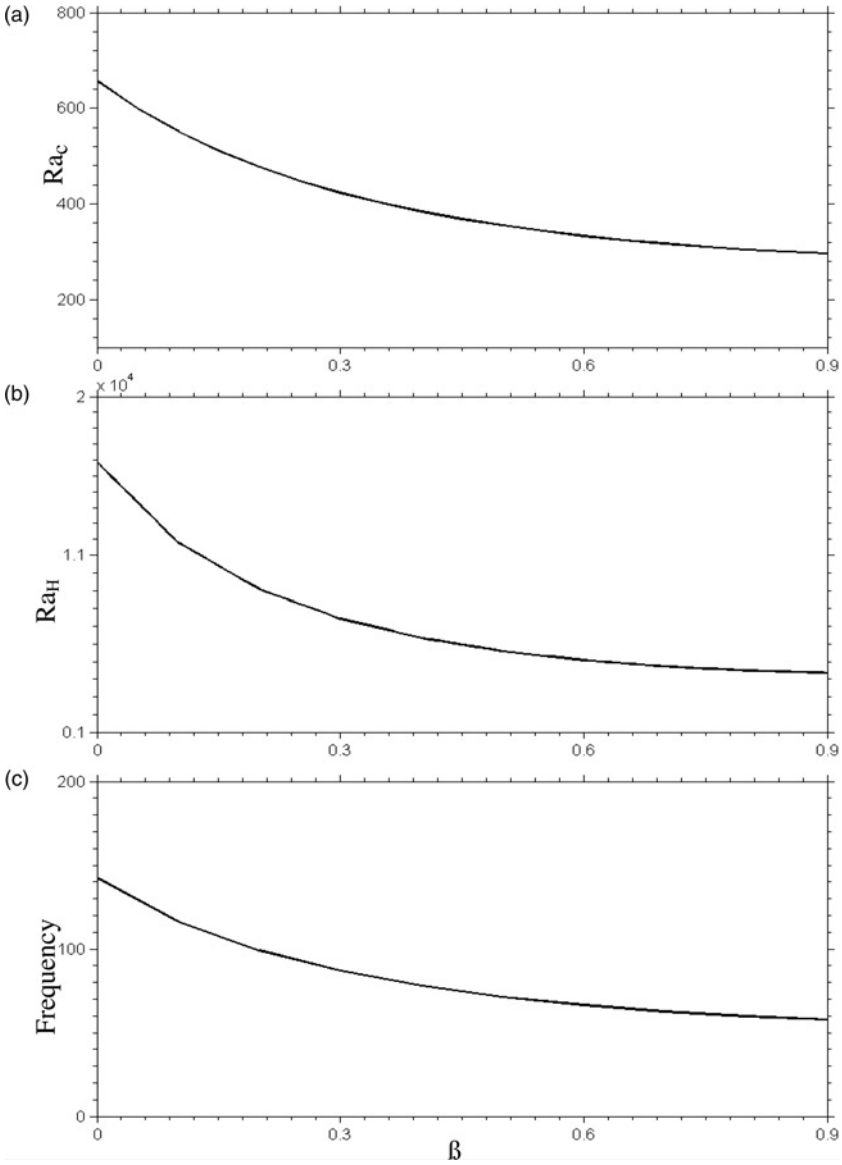

Figure 7.
Influence of modulation amplitude on the critical threshold for the onset of steady convection (Ra_C, Figure 7a), oscillatory convection (Ra_H, Figure 7b), and on the oscillatory frequency (Figure 7c), for $\alpha = 1$ and $k = \pi/\sqrt{2}$

Figure 8 on α for $\beta = 0.6$. Given the strong dependence of k_m on α and β (see later), each pattern reported in the figure is based on the corresponding k_m value. The figure shows that as α increases, the flow and temperature fields become increasingly out of phase with the domain modulation. This is particularly evident by following the warm (bright) regions, which tend to be concentrated below the crest (see the flow for $\alpha = 1$ and 2). For $\alpha = 4$, the warm and cold regions are almost both alternately beneath the crest. The velocity field in the figure suggests flow strengthening with increasing

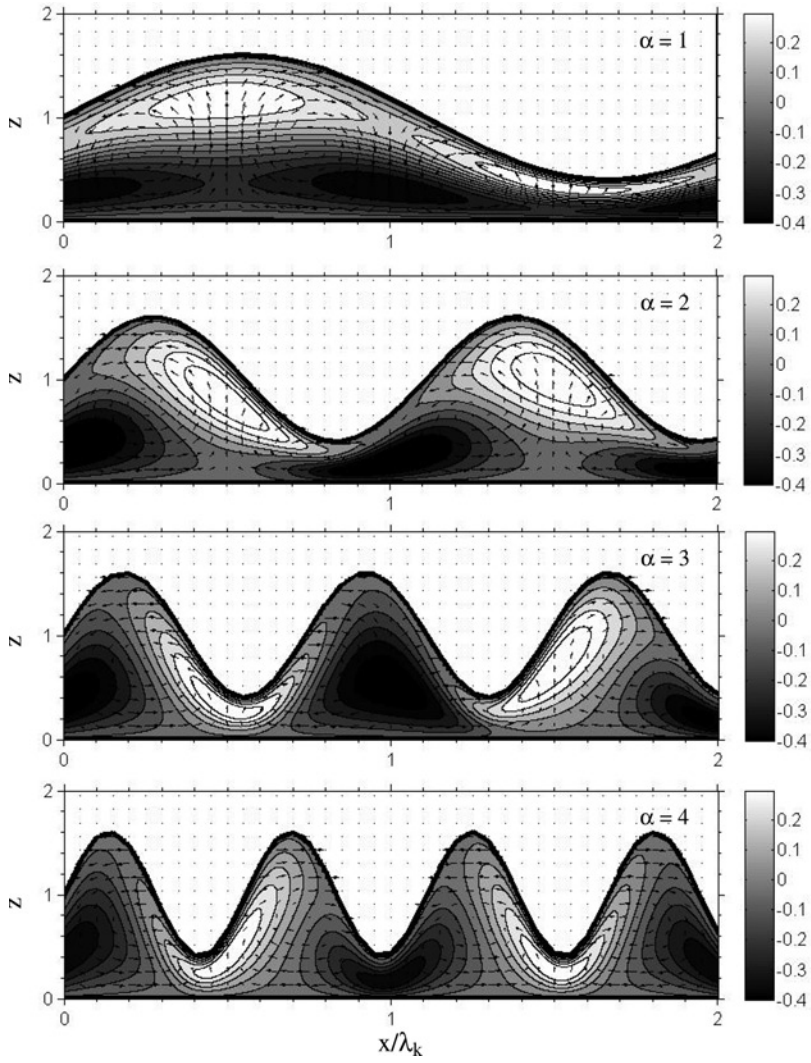

Figure 8.
Influence of modulation wavenumber α on temperature and vector fields over two disturbance wavelengths, $x \in [0, 4\pi/k]$, for $Ra = 7{,}000$, $ß = 0.6$, $Pr = 10$ and $k = k_m$

wavenumber. The velocity scale is kept the same for comparison. The case $\alpha = 4$ shows, in particular, that the flow is strongest at the modulated surface (which explains the arrows outside the flow domain). Thus, the response at low and high modulation wavenumbers can be significantly different. This is further illustrated by examining the influence of modulation amplitude on the overall rate of convection. Similarly to Figure 5, Figure 9 depicts the Nusselt number, $\langle NU(x) \rangle$, averaged over a wavelength. In this case, α is set to 2. However, in contrast to Figure 5, Figure 9 shows that the overall rate of convection tends to decrease with modulation amplitude as the critical Rayleigh number increases. Thus, whereas modulation in the case $\alpha = 1$ enhances the onset of convection, modulation tends to delay the onset of convection when α is larger than 1 (more precisely $\alpha > 1.3$ as will be shown below).

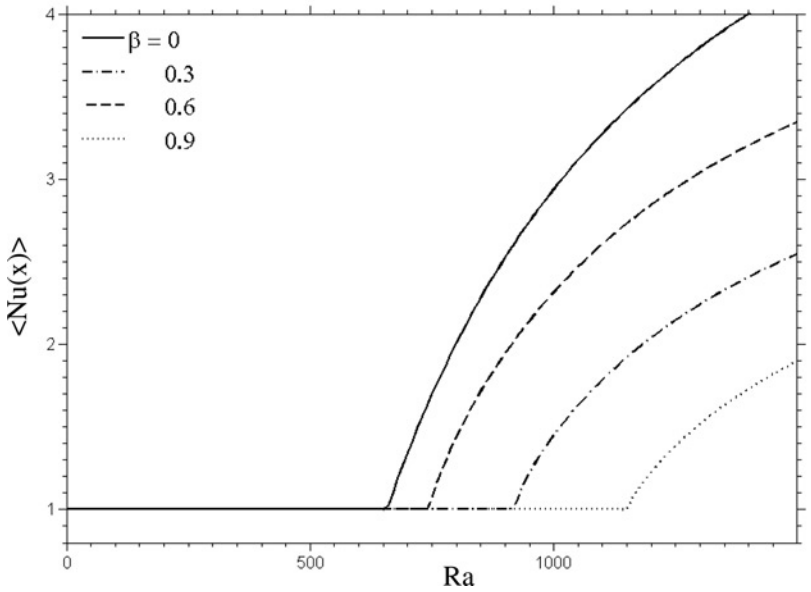

Figure 9.
Influence of modulation amplitude on the overall Nusselt number for $\alpha = 2$, $Pr = 10$ and $k = k_m$

Figure 10 shows the influence of β on the marginal stability curves for $\alpha = 2$ over relatively narrow (Figure 10a) and wide (Figure 10b) ranges of critical Rayleigh number. In contrast to the curves in Figure 6, the curves in Figure 10 indicate that both the critical Rayleigh number and corresponding disturbance wavenumber increase with β. This is a strikingly different response compared to the $\alpha = 1$ case, which seems to suggest that the onset of convection is delayed and happens over a narrower range of k values. For higher value of α, the response is even more complex, as demonstrated in Figure 11, which shows the marginal stability curves for $\beta = 0.6$. In this case, the typical parabolic shape expected for the marginal stability curve gives way to a wavy response here evident for $\alpha = 3$ and 4. The overall influence of the modulation on the stability threshold is illustrated in Figure 12, which depicts the dependence of Ra_c^m on both α and β. Typically, for a given modulation amplitude, the critical Rayleigh number tends to decrease at small α, reaches a minimum and increases essentially monotonically with α.

4. Concluding remarks

The thermal convection inside a spatially modulated channel is investigated in the present work. The governing equations are mapped onto a rectangular domain, which allows the solution to become periodic in the streamwise direction. Similarly to Rayleigh-Benard convection, conduction is lost to convection at a critical Rayleigh number. However, this critical value, Ra_C, depends strongly on both the modulation amplitude and wavenumber. For a large modulation wavelength, Ra_C decreases with modulation amplitude. Beyond a critical α value ($\alpha \approx 1.3$), Ra_C increases with modulation amplitude. Steady convection loses its stability in turn to oscillatory convection as Ra is increased further.

From a practical perspective, the study and results reported are applicable to a wide variety of problems where thermal convection occurs in variable geometry. In

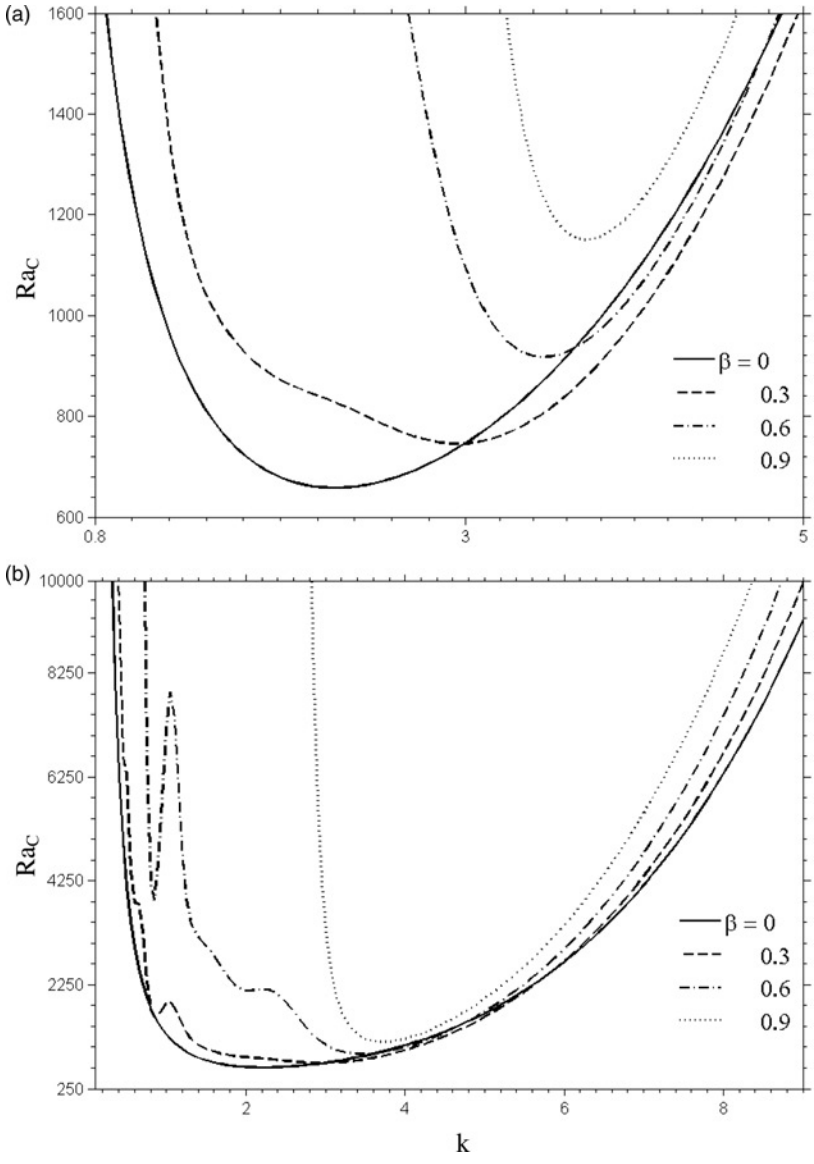

Figure 10.
Influence of modulation amplitude on the neutral stability curves over two different ranges of critical Rayleigh number (Figures 10a and b) for $\alpha = 2$

particular, the convection in heat exchangers is a prime example. The current formulation is easily extendable to other configurations, such as the modulation of both the lower and upper plates, sinusoidally or otherwise, as long as the modulation is periodic in the x direction. In this case, there is no need to alter the solution methodology, which still consists of domain mapping, spectral expansion of the velocity, pressure and temperature, Galerkin projection and solution of the projected equations.

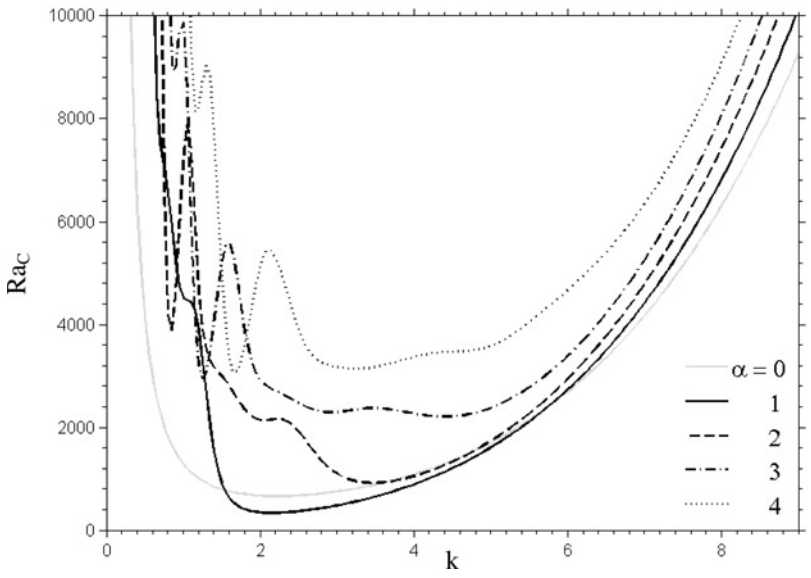

Figure 11.
Influence of modulation wavelength on the neutral stability curves, for $\beta = 0.6$

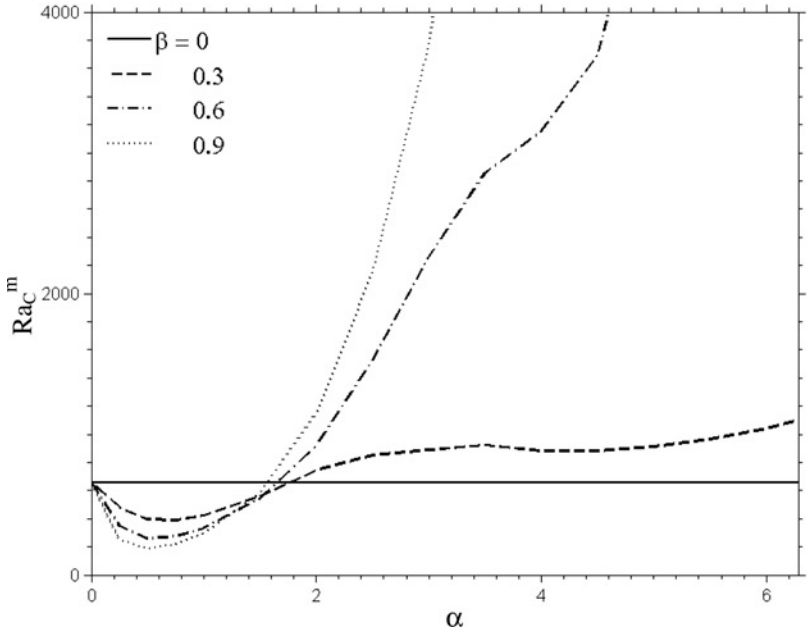

Figure 12.
Influence of the modulation amplitude on the stability threshold, $k = k_m$

References

Chen, M.N. and Whitehead, J.A. (1968), "Evolution of two-dimensional periodic Rayleigh-Bénard convection cells of arbitrary wave-numbers", *J. Fluid Mech.*, Vol. 1, p. 1.

Cross, M.C. (1988), "Structure of nonlinear traveling-wave states in finite geometries", *Phys. Rev.*, Vol. A 38, p. 3593.

Davis, S.H. (1976), "The stability of time-periodic flows", *Ann. Rev. Fluid Mech.*, Vol. 8, p. 57.

Dimitropoulos, C.D., Edwards, B.J., Kyung-Sun, C. and Beris, A.N. (1998), "Efficient pseudospectral flow simulation in moderately complex geometries", *J. Comput. Phys.*, Vol. 144, p. 517.

Drazin, P.G. and Reid, W.H. (1981), *Hydrodynamic Stability*, Cambridge University Press, Cambridge.

Kelly, R.E. and Pal, D. (1978), "Thermal convection with spatially periodic boundary conditions: resonant wavelength excitation", *J. Fluid Mech.*, Vol. 86, p. 433.

Khayat, R.E. (1999), "Finite-amplitude Taylor-vortex flow of viscoelastic fluids", *J. Fluid Mech.*, Vol. 400, p. 33.

Li, Z. and Khayat, R.E. (2004), "Pattern formation in weakly forced Taylor-Couette vortex flow", *Phys. Rev. E*, Vol. 69, p. 046305.

Ning, L. and Ecke, R.E. (1993), "Lippers-Lorentz transition at high dimensionless rotation rates in rotating Rayleigh-Bénard convection", *Phys. Rev. E*, Vol. 47, p. R2991.

Rangan, A. (2003), "Deferred correction methods for low index differential-algebraic equations", *BIT Numer. Math.*, Vol. 43, p. 1.

Schmitz, R. and Zimmerman, W. (1996a), "Spatially periodic modulated Rayleigh-Bénard convection", *Phys. Rev. E*, Vol. 53, p. 5993.

Schmitz, R. and Zimmerman, W. (1996b), "Hopf bifurcation by frustrated drifts", *Phys. Rev. E*, Vol. 53, p. R1321.

Selvarajan, S., Tulapurkara, E.G. and Vasanta Ram, V. (1999), "Stability characteristics of wavy walled channel flows", *Phys. Fluids*, Vol. 11, p. 579.

Sobey, L.J. (1980), "On the flow through furrowed channels, Part 1: calculated flow patterns", *J. Fluid Mech.*, Vol. 96, p. 1.

Stork, K. and Miller, U. (1972), "Convection in boxes: experiments", *J. Fluid Mech.*, Vol. 54, p. 599.

Szumbarski, J. and Floryan, J.M. (1999), "A direct spectral method for determination of flows over corrugated boundaries", *J. Comput. Phys.*, Vol. 153, p. 378.

Thompson, J.F., Warsi, Z.U.A. and Mastinm, C.W. (1985), *Numerical Grid Generation: Foundations and Applications*, North-Holland, New York, NY.

Tritton, D.J. (1988), *Physical Fluid Dynamics*, 2nd ed., Clarendon Press, Oxford.

Watson, A. and Poots, G. (1971), "The effects of sinusoidal protrusions on laminar free convection between vertical walls", *J. Fluid Mech.*, Vol. 49, p. 33.

Zhang, J. and Khayat, R.E. (2006), "Finite-amplitude modulated Taylor-Couette flow", *Phys. Fluids*, Vol. 18, p. 044105.

Zhou, H., Martinuzzi, R.J., Khayat, R.E. and Straatman, A.G. (2002), "On the validity of the perturbation approach for the flow inside weakly modulated channels", *Int. J. Num. Meth. Fluids*, Vol. 39, p. 1139.

Zhou, H., Martinuzzi, R.J., Khayat, R.E., Straatman, A.G. and Aburamadan, E. (2003), "Influence of modulation shape on channel flow", *Phys. Fluids*, Vol. 15, p. 3114.

Zimmerman, W., Sesselberg, M. and Petruccione, F. (1993), "Effects of disorders in pattern formation", *Phys. Rev. E*, Vol. 48, p. 2699.

Appendix. Projected equations

Upon substituting expressions (12) into Equation (7a) and projecting, one obtains:

$$\eta J_1 U^0_\eta + \eta J_6 U^c_\eta + \eta J_{11} U^s_\eta + J_2 W^0_\eta + J_7 W^c_\eta + J_{12} W^s_\eta = 0, \tag{A1a}$$

$$\pi U^s + \eta J_6 U^0_\eta + \eta J_{21} U^c_\eta + \eta J_{16} U^s_\eta + J_7 W^0_\eta + J_{22} W^c_\eta + J_{17} W^s_\eta = 0, \tag{A1b}$$

$$-\pi U^c + \eta J_{11} U^0_\eta + \eta J_{16} U^c_\eta + \eta J_{26} U^s_\eta + J_{12} W^0_\eta + J_{17} W^c_\eta + J_{27} W^s_\eta = 0. \tag{A1c}$$

Projecting the streamwise momentum Equation (7b) leads to:

$$\begin{aligned}&\frac{2\pi}{k}U^0_\tau + kU^sU^s + \eta J_1U^0U^0_\eta + J_2W^0U^0_\eta + \eta J_6U^0U^c_\eta + J_7W^0U^c_\eta + \eta J_{11}U^0U^s_\eta\\&\quad + J_{12}W^0U^s_\eta + \eta J_6U^cU^0_\eta + J_7W^cU^0_\eta + \eta J_{11}U^sU^0_\eta + J_{12}W^sU^0_\eta + \eta J_{21}U^cU^c_\eta\\&\quad + J_{22}W^cU^c_\eta + \eta J_{16}U^sU^c_\eta + J_{17}W^sU^c_\eta + \eta J_{16}U^cU^s_\eta + J_{17}W^cU^s_\eta\\&\quad + \eta J_{26}U^sU^s_\eta + J_{27}W^sU^s_\eta d\xi\\&\quad = \Pr\begin{pmatrix}\eta J_3U^0_\eta + \eta J_{51}U^c_\eta + \eta J_{52}U^s_\eta + (\eta^2J_4 + J_5)U^0_{\eta\eta} + (\eta^2J_9 + J_{10})U^c_{\eta\eta}\\ + (\eta^2J_{14} + J_{15})U^s_{\eta\eta} - \eta J_1p^0_\eta - \eta J_6p^c_\eta - \eta J_{11}p^s_\eta\end{pmatrix}\end{aligned} \tag{A2a}$$

$$\begin{aligned}&\frac{\pi}{k}U^c_\tau + \pi U^0U^s + \eta J_6U^0U^0_\eta + J_7W^0U^0_\eta + \eta J_{21}U^0U^c_\eta + J_{22}W^0U^c_\eta + \eta J_{16}U^0U^s_\eta\\&\quad + J_{17}W^0U^s_\eta + \eta J_{21}U^cU^0_\eta + J_{22}W^cU^0_\eta + \eta J_{16}U^sU^0_\eta + J_{17}W^sU^0_\eta + \eta J_{31}U^cU^c_\eta\\&\quad + J_{32}W^cU^c_\eta + \eta J_{41}U^sU^c_\eta + J_{42}W^sU^c_\eta + \eta J_{41}U^cU^s_\eta + J_{42}W^cU^s_\eta + \eta J_{46}U^sU^s_\eta\\&\quad + J_{47}W^sU^s_\eta\\&\quad = \Pr\begin{bmatrix}-k\pi U^c + \eta J_{13}U^0_\eta + \eta J_{53}U^c_\eta + \eta J_{54}U^s_\eta + (\eta^2J_9 + J_{10})U^0_{\eta\eta}\\ + (\eta^2J_{24} + J_{25})U^c_{\eta\eta} + (\eta^2J_{19} + J_{20})U^s_{\eta\eta} - \pi p^s - \eta J_6p^0_\eta\\ - \eta J_{21}p^c_\eta - \eta J_{16}p^s_\eta\end{bmatrix}\end{aligned} \tag{A2b}$$

$$\begin{aligned}&\frac{\pi}{k}U^s_\tau - \pi U^0U^c + \eta J_{11}U^0U^0_\eta + J_{12}W^0U^0_\eta + \eta J_{16}U^0U^c_\eta + J_{17}W^0U^c_\eta\\&\quad + \eta J_{26}U^0U^s_\eta + J_{27}W^0U^s_\eta + \eta J_{16}U^cU^0_\eta + J_{17}W^cU^0_\eta + \eta J_{26}U^sU^0_\eta\\&\quad + J_{27}W^sU^0_\eta + \eta J_{41}U^cU^c_\eta + J_{42}W^cU^c_\eta + \eta J_{46}U^sU^c_\eta + J_{47}W^sU^c_\eta\\&\quad + \eta J_{46}U^cU^s_\eta + J_{47}W^cU^s_\eta + \eta J_{36}U^sU^s_\eta + J_{37}W^sU^s_\eta\\&\quad = \Pr\begin{bmatrix}-k\pi U^s + \eta J_{13}U^0_\eta + \eta J_{55}U^c_\eta + \eta J_{56}U^s_\eta + (\eta^2J_{14} + J_{15})U^0_{\eta\eta}\\ + (\eta^2J_{19} + J_{20})U^c_{\eta\eta} + (\eta^2J_{29} + J_{30})U^s_{\eta\eta} + \pi p^c\\ - \eta(J_{11}p^0_\eta + J_{16}p^c_\eta + J_{26}p^s_\eta)\end{bmatrix}\end{aligned} \tag{A2c}$$

Projecting the transverse momentum Equation (7c) leads to:

$$\begin{aligned}&\frac{2\pi}{k}W^0_\tau + \pi U^cW^s - \pi U^sW^c + \eta J_1U^0W^0_\eta + \eta J_6U^cW^0_\eta + \eta J_6U^0W^c_\eta + \eta J_{21}U^cW^c_\eta\\&\quad + \eta J_{11}U^0W^s_\eta + \eta J_{16}U^cW^s_\eta + \eta J_{11}U^sW^0_\eta + J_2W^0W^0_\eta + J_7W^cW^0_\eta + J_{12}W^sW^0_\eta\\&\quad + \eta J_{16}U^sW^c_\eta + J_7W^0W^c_\eta + J_{21}W^cW^c_\eta + J_{17}W^sW^c_\eta + \eta J_{26}U^sW^s_\eta + J_{12}W^0W^s_\eta\\&\quad + J_{17}W^cW^s_\eta + J_{26}W^sW^s_\eta\\&\quad = \Pr\begin{bmatrix}\eta J_3W^0_\eta + \eta J_{51}W^c_\eta + \eta J_{52}W^s_\eta + (\eta^2J_4 + J_5)W^0_{\eta\eta} + (\eta^2J_9 + J_{10})W^c_{\eta\eta}\\ + (\eta^2J_{14} + J_{15})W^s_{\eta\eta} - J_2p^0_\eta - J_7p^c_\eta - J_{12}p^s_\eta + Ra\left(\frac{2\pi}{k}\theta^0\right)\end{bmatrix}\end{aligned} \tag{A3a}$$

$$\begin{aligned}
&\frac{\pi}{k}W^c_\tau + \pi U^0 W^s + \eta J_6 U^0 W^0_\eta + \eta J_{21} U^c W^0_\eta + \eta J_{21} U^0 W^c_\eta + \eta J_{31} U^c W^c_\eta + \eta J_{16} U^0 W^s_\eta \\
&\quad + \eta J_{41} U^c W^s_\eta + \eta J_{16} U^s W^0_\eta + J_7 W^0 W^0_\eta + J_{22} W^c W^0_\eta + J_{17} W^s W^0_\eta + \eta J_{41} U^s W^c_\eta \\
&\quad + J_{22} W^0 W^c_\eta + J_{32} W^c W^c_\eta + J_{42} W^s W^c_\eta + \eta J_{46} U^s W^s_\eta + J_{17} W^0 W^s_\eta + J_{42} W^c W^s_\eta \\
&\quad + J_{47} W^s W^s_\eta \qquad \text{(A3b)} \\
&\qquad = \mathrm{Pr}\begin{bmatrix} -k\pi W^c + \eta J_8 W^0_\eta + \eta J_{53} W^c_\eta + \eta J_{54} W^s_\eta + (\eta^2 J_9 + J_{10}) W^0_{\eta\eta} \\ + (\eta^2 J_{24} + J_{25}) W^c_{\eta\eta} + (\eta^2 J_{19} + J_{20}) W^s_{\eta\eta} - J_7 p^0_\eta - J_{22} p^c_\eta \\ - J_{17} p^s_\eta + \mathrm{Ra}\left(\frac{\pi}{k}\theta^c\right) \end{bmatrix}
\end{aligned}$$

$$\begin{aligned}
&\frac{\pi}{k}W^s_\tau - \pi U^0 W^c + \eta J_{11} U^0 W^0_\eta + \eta J_{16} U^c W^0_\eta + \eta J_{16} U^0 W^c_\eta + \eta J_{41} U^c W^c_\eta + \eta J_{26} U^0 W^s_\eta \\
&\quad + \eta J_{46} U^c W^s_\eta + \eta J_{26} U^s W^0_\eta + J_{12} W^0 W^0_\eta + J_{17} W^c W^0_\eta + J_{27} W^s W^0_\eta \\
&\quad + \eta J_{46} U^s W^c_\eta + J_{17} W^0 W^c_\eta + J_{42} W^c W^c_\eta + J_{47} W^s W^c_\eta + \eta J_{36} U^s W^s_\eta + J_{27} W^0 W^s_\eta \\
&\quad + J_{47} W^c W^s_\eta + J_{37} W^s W^s_\eta \qquad \text{(A3c)} \\
&\qquad = \mathrm{Pr}\begin{bmatrix} -k\pi W^s + \eta J_{13} W^0_\eta + \eta J_{55} W^c_\eta + \eta J_{56} W^s_\eta + (\eta^2 J_{14} + J_{15}) W^0_{\eta\eta} \\ + (\eta^2 J_{19} + J_{20}) W^c_{\eta\eta} + (\eta^2 J_{29} + J_{30}) W^s_{\eta\eta} - J_{12} p^0_\eta - J_{17} p^c_\eta \\ - J_{27} p^s_\eta + \mathrm{Ra}\left(\frac{\pi}{k}\theta^s\right) \end{bmatrix}
\end{aligned}$$

Projecting the energy Equation (7c) leads to:

$$\begin{aligned}
&\frac{2\pi}{k}\theta^0_\tau - \pi U^s \theta^c + \pi U^c \theta^s + \eta J_1 U^0 \theta^0_\eta + \eta J_6 U^c \theta^0_\eta + \eta J_{11} U^s \theta^0_\eta + J_2 W^0 \theta^0_\eta + J_7 W^c \theta^0_\eta \\
&\quad + J_{12} W^s \theta^0_\eta + \eta J_6 U^0 \theta^c_\eta + \eta J_{21} U^c \theta^c_\eta + \eta J_{16} U^s \theta^c_\eta + J_7 W^0 \theta^c_\eta \\
&\quad + J_{22} W^c \theta^c_\eta + J_{17} W^s \theta^c_\eta + \eta J_{11} U^0 \theta^s_\eta + \eta J_{16} U^c \theta^s_\eta + \eta J_{26} U^s \theta^s_\eta + J_{12} W^0 \theta^s_\eta \\
&\quad + J_{17} W^c \theta^s_\eta + J_{26} W^s \theta^s_\eta \\
&\quad + (-\alpha A^1 J_{63} + \alpha B^1 J_{57} + \eta A^0_\eta J_1 + \eta A^1_\eta J_{69} + \eta B^1_\eta J_{75}) U^0 \\
&\quad + (-\alpha A^1 J_{64} + \alpha B^1 J_{58} + \eta A^0_\eta J_6 + \eta A^1_\eta J_{70} + \eta B^1_\eta J_{76}) U^c \qquad \text{(A4a)} \\
&\quad + (-\alpha A^1 J_{66} + \alpha B^1 J_{60} + \eta A^0_\eta J_{11} + \eta A^1_\eta J_{71} + \eta B^1_\eta J_{77}) U^s \\
&\quad + (A^0_\eta J_2 + A^1_\eta J_{81} + B^1_\eta J_{87}) W^0 + (A^0_\eta J_7 + A^1_\eta J_{82} + B^1_\eta J_{88}) W^c \\
&\quad + (A^0_\eta J_{12} + A^1_\eta J_{83} + B^1_\eta J_{89}) W^s \\
&\qquad = \eta J_3 \theta^0_\eta + \eta J_{51} \theta^c_\eta + \eta J_{52} \theta^s_\eta + (\eta^2 J_4 + J_5) \theta^0_{\eta\eta} + (\eta^2 J_9 + J_{10}) \theta^c_{\eta\eta} \\
&\qquad\quad + (\eta^2 J_{14} + J_{15}) \theta^s_{\eta\eta}
\end{aligned}$$

$$\begin{aligned}
&\frac{\pi}{k}\theta^c_\tau + \pi U^0 \theta^s + \eta J_6 U^0 \theta^0_\eta + \eta J_{21} U^c \theta^0_\eta + \eta J_{16} U^s \theta^0_\eta + J_{12} W^0 \theta^0_\eta + J_{22} W^c \theta^0_\eta + J_{17} W^s \theta^0_\eta \\
&\quad + \eta J_{21} U^0 \theta^c_\eta + \eta J_{31} U^c \theta^c_\eta + \eta J_{41} U^s \theta^c_\eta + J_{22} W^0 \theta^c_\eta + J_{32} W^c \theta^c_\eta + J_{42} W^s \theta^c_\eta \\
&\quad + \eta J_{16} U^0 \theta^s_\eta + \eta J_{41} U^c \theta^s_\eta + \eta J_{46} U^s \theta^s_\eta + J_{17} W^0 \theta^s_\eta + J_{42} W^c \theta^s_\eta + J_{47} W^s \theta^s_\eta \\
&\quad (-\alpha A^1 J_{64} + \alpha B^1 J_{58} + \eta A^0_\eta J_6 + \eta A^1_\eta J_{70} + \eta B^1_\eta J_{76}) U^0
\end{aligned}$$

$$
\begin{aligned}
&+(-\alpha A^1 J_{67}+\alpha B^1 J_{61}+\eta A^0_\eta J_{21}+\eta A^1_\eta J_{73}+\eta B^1_\eta J_{79})U^c\\
&+(-\alpha A^1 J_{66}+\alpha B^1 J_{60}+\eta A^0_\eta J_{16}+\eta A^1_\eta J_{72}+\eta B^1_\eta J_{78})U^s\\
&+(A^0_\eta J_7+A^1_\eta J_{82}+B^1_\eta J_{88})W^0+(A^0_\eta J_{22}+A^1_\eta J_{85}+B^1_\eta J_{91})W^c\\
&+(A^0_\eta J_{17}+A^1_\eta J_{84}+B^1_\eta J_{90})W^s\\
&\quad=-k\pi\theta^c+\eta J_8\theta^0_\eta+\eta J_{53}\theta^c_\eta+\eta J_{54}\theta^s_\eta+(\eta^2 J_9+J_{10})\theta^0_{\eta\eta}+(\eta^2 J_{24}+J_{25})\theta^c_{\eta\eta}\\
&\qquad+(\eta^2 J_{19}+J_{20})\theta^s_{\eta\eta}
\end{aligned}
\tag{A4b}
$$

$$
\begin{aligned}
&\frac{\pi}{k}\theta^s_\tau-\pi U^0\theta^c+\eta J_{11}U^0\theta^0_\eta+\eta J_{16}U^c\theta^0_\eta+\eta J_{26}U^s\theta^0_\eta+J_{12}W^0\theta^0_\eta+J_{17}W^c\theta^0_\eta+J_{27}W^s\theta^0_\eta\\
&\quad+\eta J_{16}U^0\theta^c_\eta+\eta J_{41}U^c\theta^c_\eta+\eta J_{46}U^s\theta^c_\eta+J_{17}W^0\theta^c_\eta+J_{42}W^c\theta^c_\eta+J_{47}W^s\theta^c_\eta\\
&\quad+\eta J_{26}U^0\theta^s_\eta+\eta J_{46}U^c\theta^s_\eta+\eta J_{36}U^s\theta^s_\eta+J_{27}W^0\theta^s_\eta+J_{47}W^c\theta^s_\eta+J_{37}W^s\theta^s_\eta\\
&\quad+(-\alpha A^1 J_{65}+\alpha B^1 J_{59}+\eta A^0_\eta J_{11}+\eta A^1_\eta J_{71}+\eta B^1_\eta J_{77})U^0\\
&\quad+(-\alpha A^1 J_{66}+\alpha B^1 J_{60}+\eta A^0_\eta J_{16}+\eta A^1_\eta J_{72}+\eta B^1_\eta J_{78})U^c\\
&\quad+(-\alpha A^1 J_{68}+\alpha B^1 J_{62}+\eta A^0_\eta J_{26}+\eta A^1_\eta J_{74}+\eta B^1_\eta J_{80})U^s\\
&\quad+(A^0_\eta J_{12}+A^1_\eta J_{83}+B^1_\eta J_{89})W^0+(A^0_\eta J_{17}+A^1_\eta J_{84}+B^1_\eta J_{90})W^c\\
&\quad+(A^0_\eta J_{27}+A^1_\eta J_{86}+B^1_\eta J_{92})W^s\\
&\qquad=-k\pi\theta^s+\eta J_{13}\theta^0_\eta+\eta J_{55}\theta^c_\eta+\eta J_{56}\theta^s_\eta+(\eta^2 J_{14}+J_{15})\theta^0_{\eta\eta}\\
&\qquad+(\eta^2 J_{19}+J_{20})\theta^c_{\eta\eta}+(\eta^2 J_{29}+J_{30})\theta^s_{\eta\eta}
\end{aligned}
\tag{A4c}
$$

The coefficients $J_1, J_2, \ldots$ are constants.

Corresponding author
Roger E. Khayat can be contacted at: rkhayat@uwo.ca